Ion-pair dissociation of highly excited carbon clusters: Size and charge effects

Thibaut Launoy, Karine Béroff, Marin Chabot, Guillaume Martinet, Arnaud Le Padellec, Thomas Pino, Sandra Bouneau, Nathalie Vaeck, Jacques Liévin, Géraldine Féraud, et al.

Ion-pair dissociation of highly excited carbon clusters: Size and charge effects

Thibaut Launoy,[1,*] Karine Béroff,[2,†] Marin Chabot,[3] Guillaume Martinet,[3] Arnaud Le Padellec,[4] Thomas Pino,[2] Sandra Bouneau,[3] Nathalie Vaeck,[1] Jacques Liévin,[1] Géraldine Féraud,[2,‡] Jérôme Loreau,[1] and Thejus Mahajan[2]

[1]*Laboratoire de Chimie Quantique et Photophysique (CQP) Université Libre de Bruxelles (ULB) CP160/09 1050 Bruxelles, Belgium*

[2]*Institut des Sciences Moléculaires d'Orsay (ISMO) CNRS-INP Univ. Paris-Sud Univ. Paris-Saclay F-91405 Orsay, France*

[3]*Institut de Physique Nucléaire d'Orsay (IPNO) CNRS-I2NP3 Univ. Paris-Sud Univ. Paris-Saclay F-91406 Orsay, France*

[4]*Institut de Recherche en Astrophysique et Planétologie (IRAP) CNRS-INP Univ. Toulouse 3 F-31028 Toulouse, France*

(Received 21 July 2016; revised manuscript received 4 November 2016; published 13 February 2017)

We present measurements of ion-pair dissociation (IPD) of highly excited neutral and ionized carbon clusters $C_{n=2-5}^{(q=0-3)+}$. The tool for producing these species was a high-velocity collision between C_n^+ projectiles ($v = 2.25$ a.u.) and helium atoms. The setup allowed us to detect in coincidence anionic and cationic fragments, event by event, leading to a direct and unambiguous identification of the IPD process. Compared with dissociation without anion emission, we found typical 10^{-4} IPD rates, not depending much on the size and charge of the (n,q) species. Exceptions were observed for C_2^+ and, to a lesser extent, C_4^{3+} whose IPDs were notably lower. We tentatively interpret IPDs of C_2^+ and C_3^+ by using a statistical approach based on the counting of final states allowed by energetic criteria. The model is able to furnish the right order of magnitude for the experimental IPD rates and to provide a qualitative explanation of the lower IPD rate observed in C_2^+.

DOI: 10.1103/PhysRevA.95.022711

I. INTRODUCTION

Ion-pair dissociation (IPD) is a relaxation process of highly excited molecules proceeding through emission of an anionic and one (or several) cationic fragments. IPD was observed long ago in mass spectrometric studies of diatomic molecules [1] and has been mostly studied following photoexcitation by vacuum ultraviolet (VUV) [2,3] or soft-x-ray [4] radiation. IPD was also observed following recombination of low-energy electrons with molecular cations, a resonant process competitive with dissociative recombination [5], and also in collisions between molecular ions and atoms in low- [6] and high-velocity [7–9] collisions. It is noticeable that IPD, which requires electron excitation into highly excited states, is also observed in low-velocity collisions [6]. Interestingly, it was recently shown that, in low-velocity collisions, the anionic fragment production by nuclear two-body interaction is minor as compared with the production arising from electron excitation [10]. Most of the work on IPD has been devoted to the case of neutral molecules giving rise to one anion and one singly charged fragment. Following the pioneering work of Dujardin *et al.* [11] it was shown that emission of two singly charged fragments or one doubly charged fragment together with one anion was also possible, and was indeed the rule in the case of photoexcitation in inner shells due to the Auger effect [12,13]. IPD associating three positive charges together with one negative charge has been suspected [14] although never directly identified.

Two formation mechanisms of IPD, direct and indirect, have been proposed. The direct mechanism, population of a state dissociating at infinite internuclear distances towards an ion-pair limit, is not expected to be very probable because excitation in the Franck Condon (FC) region has to occur in the repulsive inner wall of the potential-energy profile [4]. It is nevertheless possible, as recently observed in photoexcitation of O_2 by absorption of three UV photons within a fs laser pulse [15]. The indirect population is expected to occur by coupling between the ion-pair state and a highly vibrationally excited Rydberg or cationic state of the molecule populated in the FC region. It was often demonstrated through the observation of vibrational progressions in the fragment spectra [16]. The mechanism may also depend on the dynamics of excitation, i.e., the absorption of one or several photons [16,17]. In addition to these two mechanisms one has to take into account the crossings between molecular states at large internuclear distances [15] which may populate or depopulate an ion-pair dissociation limit and makes the description and following of the IPD process very complicated. Note that the three pathways to IPD (direct, indirect, and crossings at large internuclear distances) all involve very excited electronic states.

Despite these numerous works there are still many unknowns concerning the IPD process. The yield of IPD is found to vary strongly from one work to another and it is not clear what is governing the values obtained. By the way, this yield is sometimes referenced to the ionization [16], sometimes to the total fragmentation [9], and sometimes to another process [5]. As mentioned before, only a few works have reported on IPD with three positive charges and no results were obtained, to our knowledge, for four positive charges.

In this paper we present measurements of ion-pair relaxation of highly excited neutral and ionized carbon clusters $C_{n=2-5}^{q+=0-3}$. The tool for producing these species was a high velocity collision between C_n^+ projectiles ($v = 2.25$ a.u.) and helium atoms. The setup allowed us to detect in coincidence anionic and cationic fragments, event by event, leading to a direct and unambiguous identification of the IPD process. Moreover, we measured ion-pair dissociation of carbon clusters in different charge states $q = 0$–3, allowing a study of size and charge effects. In particular, we observed IPD associated with emission of four positive charges together

*tlaunoy@ulb.ac.be

†karine.beroff@u-psud.fr

‡Present address: LERMA, Sorbonne Universités UPMC Univ. Paris 06, Observatoire de Paris, PSL Research University, CNRS F-75252 Paris, France.

with one negative charge. Finally, we made an attempt to interpret some of IPD rates within a statistical approach. Due to crude approximations it is expected to furnish no more than an order-of-magnitude estimate of the process. Still, it constitutes a rare case of interpretation of absolute IPD measurements in the literature.

The plan of the paper is as follows: In Sec. II, we describe the experimental setup and methods used to extract IPD probabilities; namely, coincidence measurements, in order to identify the process and target density-dependence study to remove contributions from double collisions. In Sec. III, we present results concerning the IPD probabilities, rates, and cross sections for C_n^{q+} as a function of n and q. IPD rates are tentatively interpreted in Sec. IV for the case of C_2^+ and C_3^+ in the frame of a simple statistical approach. We conclude in Sec. V.

II. EXPERIMENT

The experiment was done at the Tandem accelerator in Orsay by using a dedicated setup (AGAT) described below. The setup is the same as that described in Ref. [18]. Briefly, C_n^+ projectiles of 125 keV/u energy (constant velocity of 2.25 a.u.) were delivered by the accelerator and sent to the AGAT setup consisting of a collision chamber, a fragment electrostatic analyzer, and a fragment-detection chamber. In the collision chamber, the C_n^+ projectiles traverse a low-density helium gaseous jet whose thickness, $n\delta x$, could be varied by changing the flow rate through the formation capillary [19]. In the electrostatic analyzer chamber, projectiles and fragments were deflected according to their charge-over-mass ratios thanks to the application of a strong electric field of a few tens of kV/cm produced between two parallel plates. In the detection chamber six or seven solid-state silicon detectors were positioned to intercept negatively charged, neutral, and positively charged fragments. The current signals issued from the detectors were used to extract the masses of the fragments and allowed to resolve pileup events associated with the impact of many fragments in the same detector (in the case of the neutral fragment detector, for instance [20]). With these methods all fragments were detected (100% efficiency, 4π detection in the projectile frame) and identified with respect to their mass *and* charge. In some of the experiments the detector of neutral fragments was replaced by an original position sensitive CCD camera [21]. With this detector, we extracted the dissociative kinetic energy of the C fragment following dissociation of C_2^{q+} into C^{q+} and C [22].

Whereas typical target thicknesses (a few 10^{13} atoms/cm^2) guaranteed the single-collision condition for all major processes (electronic excitation, ionization, single electron capture) this was not the case for processes of very small cross sections such as double electron capture [18] and ion-pair dissociation. For these processes of very small cross sections, double collisions compete with single collisions and have to be subtracted. This was done by performing a target-thickness dependence of the *normalized* probabilities (which are constant or linear with $n\delta x$ depending on whether this is a single- or double-collision process), as explained in Ref. [18] [see Eqs. (1)–(4) in that reference]. Figure 1 illustrates the method in the case of the C_2^--C_2^+-C^+ channel whose production probability, normalized to the total excitation and ionization probability of C_5^+, is plotted as a function of the helium target thickness $n\delta x$. The value of the ordinate at zero thickness is used to extract the C_2^--C_2^+-C^+ channel *due to IPD*.

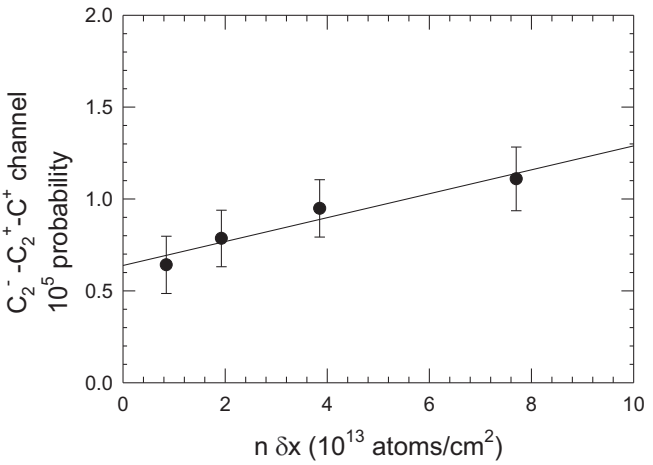

FIG. 1. Measured C_2^--C_2^+-C^+ production probability normalized to the total excitation and ionization probability of C_5^+ as a function of the helium target thickness $n\delta x$ (C_5^+-He collision at $v = 2.25$ a.u). The value at zero thickness is used to extract the C_2^--C_2^+-C^+ channel due to IPD.

In the following we present various experimental observables. Measured probabilities for IPD as compared with total dissociation of the C_n^{q+} species are presented for all IPD channels and all C_n^{q+} species in Table I ($n = 2$–3) and Table II ($n = 4$–5). By summing values for all channels within an (n,q) species we obtain the total IPD rate of the C_n^{q+} species, which is denoted $R_{\rm IPD}(C_n^{q+})$, and presented in bold in the Tables I and II. For instance, in the case of dissociation following electronic excitation of C_2^+ (dissociative excitation), $R_{\rm IPD}(C_2^+)$ writes

$$R_{\rm IPD}(C_2^+) = \frac{p(C^{2+}\text{-}C^-)}{p(C^+\text{-}C) + p(C^{2+}\text{-}C^-)}, \tag{1}$$

where $p(C^{2+}\text{-}C^-)$ and $p(C^+\text{-}C)$ are the measured C^{2+}-C^- and C^+-C channel occurrence probabilities per incident C_2^+. These quantities are related to the dissociative excitation cross section $\sigma_{\rm exc.diss}$ by

$$p(C^{2+}\text{-}C^-) = \sigma_{\rm exc.diss}\, n\delta x\, R_{\rm IPD}(C_2^+), \tag{2}$$

$$p(C^+\text{-}C) = \sigma_{\rm exc.diss}\, n\delta x\, [1 - R_{\rm IPD}(C_2^+)]. \tag{3}$$

In the case of C_3^+, two $R_{\rm IPD}$ values were extracted whose expressions are given in Eqs. (4) and (5). The $R_{\rm IPD,1}$ quantity [Eq. (4)] refers to the generic definition of $R_{\rm IPD}$ given above. For simplicity, the $R_{\rm IPD,2}$ quantity, associated with normalization of IPD to three-fragment dissociation only [see denominator in Eq. (5)], is the one interpreted in Sec. IV:

$$R_{\rm IPD,1}(C_3^+) = \frac{p(C^-\text{-}C^+\text{-}C^+)}{p(C_2^+\text{-}C) + p(C^+\text{-}C\text{-}C) + p(C^-\text{-}C^+\text{-}C^+)}, \tag{4}$$

$$R_{\rm IPD,2}(C_3^+) = \frac{p(C^-\text{-}C^+\text{-}C^+)}{p(C^+\text{-}C\text{-}C) + p(C^-\text{-}C^+\text{-}C^+)}. \tag{5}$$

TABLE I. Measured IPD probabilities (column 3) in individual channels (column 2) of C_n^{q+} species (n, q given in column 1), normalized to the total dissociation probability of the species. Values reported in bold in column 3 correspond to R_{IPD} obtained by summing individual probabilities within an (n,q) species. For ($n = 3$, $q = 1$), the two values correspond to $R_{\mathrm{IPD},1}$ and $R_{\mathrm{IPD},2}$ whose expressions have been given in Eqs. (4) and (5). In column 4 are reported branching ratios for dissociation along a particular ion-pair channel within (n,q). The energy cost of each channel is reported in column 5.

n, q	Channel	Ion-pair dissociation probability (abs. err)	Branching ratio within ion-pair dissociation (abs. err)	Energy above the ground state of C_n^{q+} (eV)
2, 0	C^--C^+	**5.43(0.65)**$\times10^{-4}$	1	16.1
2, 1	C^--C^{2+}	**2.94(1.62)**$\times10^{-5}$	1	28.5
3, 0	C_2^--C^+	4.29(0.53)$\times10^{-4}$	0.58(0.07)	15.7
	C^--C^+-C	1.91(0.50)$\times10^{-4}$	0.26(0.07)	23.9
	C^--C_2^+	1.20(0.32)$\times10^{-4}$	0.16(0.04)	18.2
		7.40(0.8)$\times10^{-4}$		
3, 1	C^--$2C^+$	**2.90(0.2)**$\times10^{-4}$	1	23.2
		5.30(1.5)$\times10^{-4}$	1	

TABLE II. Same as Table I but for $n = 4$–5.

n, q	Channel	Ion-pair dissociation probability (abs. err)	Branching ratio within ion-pair dissociation (abs. err)	Energy above the ground state of C_n^{q+}(eV)
4, 0	C^--C_2-C^+	6.10(3.5)$\times10^{-5}$	0.36(0.19)	22.9
	C_2^--C-C^+	5.07(3.3)$\times10^{-5}$	0.30(0.18)	20.9
	C_2^--C_2^+	3.47(2.0)$\times10^{-5}$	0.20(0.11)	15.5
	C_3^--C^+	2.40(2.0)$\times10^{-5}$	0.14(0.11)	14.6
		1.70(0.56)$\times10^{-4}$		
4, 1	C^--C-$2C^+$	1.53(0.22)$\times10^{-4}$	0.53(0.07)	28.5
	C^--C_2^+-C^+	7.09(1.3)$\times10^{-5}$	0.25(0.04)	23.0
	C_2^--$2C^+$	6.33(1.19)$\times10^{-5}$	0.22(0.04)	20.4
		2.90(0.28)$\times10^{-4}$		
4, 2	C^--$3C^+$	1.57(0.14)$\times10^{-4}$	0.96(0.01)	22.4
	C^--C^{2+}-C^+-C[a]	6.0(0.6)$\times10^{-6}$	0.04(0.01)	35.5
		1.60(0.14)$\times10^{-4}$		
4, 3	C^--$2C^+$-C^{2+}[a]	7.31(2.12)$\times10^{-5}$	0.96(0.03)	38.1
	C^--C-$2C^{2+}$[a]	2.58(2.05)$\times10^{-6}$	0.04(0.03)	39.9
		7.60(2.10)$\times10^{-5}$		
5, 0	C_2^--C_3^+	4.9(2.0)$\times10^{-5}$	0.42(0.16)	14.5
	C_2^--C_2-C^+	3.6(1.5)$\times10^{-5}$	0.31(0.13)	21.0
	C_2^--C_2^+-C	3.2(1.5)$\times10^{-5}$	0.27(0.13)	21.8
		1.18(0.29)$\times10^{-4}$		
5,1	C_2^--$2C^+$-C	5.78(0.97)$\times10^{-5}$	0.30(0.05)	28
	C^--2C-$2C^+$	5.67(1.11)$\times10^{-5}$	0.29(0.06)	36
	C^--C-C^+-C_2^+	2.91(0.8)$\times10^{-5}$	0.15(0.04)	30.3
	C_2^--C_2^+-C^+	2.33(0.5)$\times10^{-5}$	0.12(0.03)	22.5
	C^--C_2-$2C^+$	2.0(0.6)$\times10^{-5}$	0.10(0.03)	30
	C_3^--$2C^+$	8.0(3.2)$\times10^{-6}$	0.04(0.02)	21.1
		1.95(0.20)$\times10^{-4}$		
5, 2	C^--C-$3C^+$	1.56(0.24)$\times10^{-4}$	0.67(0.10)	31
	C_2^--$3C^+$	3.96(0.77)$\times10^{-5}$	0.17(0.03)	21.7
	C^--C_2^+-$2C^+$	3.59(0.77)$\times10^{-5}$	0.16(0.03)	25.4
		2.31(0.26)$\times10^{-4}$		
5, 3	C^--$4C^+$	**3.95(0.53)**$\times10^{-4}$	1	17.6

[a]Measurements performed at $v = 2.6$ a.u.

Also presented in the next section are IPD cross sections $\sigma((q+1)+,-)$ which are defined as

$$\sigma((q+1)+,-) = \sigma_{\rm diss}\left(C_n^{q+}\right) R_{\rm IPD}\left(C_n^{q+}\right), \tag{6}$$

where $\sigma_{\rm diss}(C_n^{q+})$ refers to the total dissociation cross section of C_n^{q+}. Note that the notation $((q+1)+,-)$ means fragmentation into one anion and one or several cations whose total positive charge is $(q+1)$.

III. EXPERIMENTAL RESULTS FOR ION-PAIR PROBABILITIES, RATES AND CROSS SECTIONS

In Tables I and II are reported measured IPD probabilities (column 3) in individual channels (column 2) of C_n^{q+} species (n, q given in column 1), normalized to the total dissociation probability of the species. Values reported in bold in column 3 correspond to $R_{\rm IPD}$ (IPD rates) obtained by summing individual probabilities within an (n,q) species. For $(n=3,\ q=1)$, the two bold values correspond to $R_{\rm IPD,1}$ and $R_{\rm IPD,2}$ whose expressions have been given in Eqs. (4) and (5) and that differ by the normalization (denominator). In column 4 are reported branching ratios for dissociation along a particular ion-pair channel within (n,q). Column 5 gives the energy cost of each channel. This last quantity is defined as the minimum energy that the C_n^{q+} species must possess above its ground state to dissociate along the channel. It was obtained from calculated dissociation energies of C_n^{q+} clusters [23,24], using electron affinities of C_n^- [25] and assuming no barriers to the dissociation.[1]

It is readily seen that the IPD process is a very small part of the total dissociation, $R_{\rm IPD}$ values ranging from a few 10^{-5} to a few 10^{-4}. It is interesting to remark that, for C_3^+, we find an $R_{\rm IPD}$ value close to (three times smaller) the one obtained for H_3^+ in a similar collision system (H_3^+-He at $v=1.4$ a.u) [9]. We comment on this result in Sec. IV. An important quantity that governs the probability of relaxation by a given process is the energy it requires. As seen in the last column of Tables I and II, the energy cost of IPD is rather high: from 14 up to 40 eV depending on the channel. Also, the more probable ion-pair channels are usually not those reachable with the lowest energy. For instance, three-fragment channels, despite large error bars, seem more probable than two-fragment channels for $q=0$ and $n=4$ (see top of Fig. 2) whereas four and five-fragments channels are more probable than three-fragments channels for $q=1$ and $n=5$ (see bottom of Fig. 2). This indicates that IPD involves highly excited states. Indeed, in a statistical fragmentation context, species with high internal energies tend to relax by fragment production rather than by furnishing more kinetic or vibrational energy to few fragments [28]. Within two-fragments channels, i.e., within a given internal energy domain, we note that the molecular anion C_2^- is more often present than C^- or C_3^- which is in agreement with electron affinities of these species, respectively equal to 3.4, 1.3, and 2 eV [25].

Figure 3 presents measured IPD cross sections $\sigma((q+1)+,-)$ of C_n^{q+} clusters as a function of the cluster size n and for

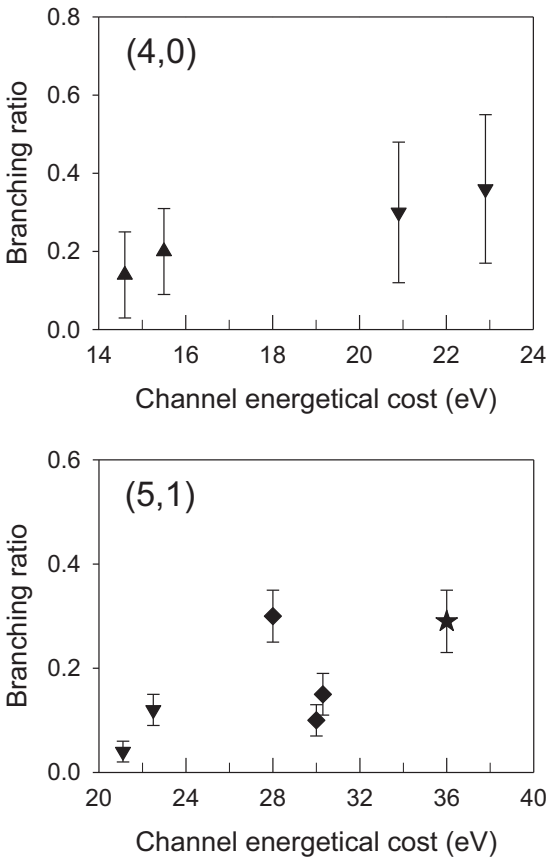

FIG. 2. Measured branching ratios for ion-pair channels in C_4 ($n=4$, $q=0$, top panel) and C_5^+ ($n=5$, $q=1$ bottom panel) as a function of the energy cost (eV). Upward triangles, downward triangles, diamonds, and star correspond respectively to two-fragment, three-fragment, four-fragment, and five-fragment IPD channels.

various values of q ($q=0$ to $q=3$ from top-left to bottom-right panel of Fig. 3). These cross sections have typical values between 10^{-20} and 10^{-19} cm^2 with some notable exceptions for C_2^+ (2.9×10^{-21} cm^2) and, to a lesser extent, C_4^{3+} (8.6×10^{-21} cm^2). Apart from these two singularities we observe a tendency of IPD cross sections, weakly dependent on n, to rise with q (from $q=0$ up to $q=2$) and then to decrease again at $q=3$. According to Eq. (6) this can originate from $\sigma_{\rm diss}$ or from $R_{\rm IPD}$. It can be shown from previous studies [29,30] that $\sigma_{\rm diss}$ follow this tendency so that a rather constant dependence of $R_{\rm IPD}$ with q is to be expected. This is what is mainly observed in Fig. 4 with the two exceptions of C_2^+ and C_4^{3+} species. In particular, the $R_{\rm IPD}$ value obtained for C_2^+ is roughly ten times smaller that all other $q=1$ $R_{\rm IPD}$s. The origin of this difference is tentatively interpreted in Sec. IV by comparing, within a statistical approach, $R_{\rm IPD}$ predicted for C_2^+ and C_3^+.

IV. TENTATIVE INTERPRETATION OF ION-PAIR-DISSOCIATION RATES IN C_2^+ AND C_3^+

Multiconfigurational *ab initio* calculations have been performed on the C_2^+ cation in order to investigate the energy pattern of the potential-energy curves (PECs) up to the first ion-pair-dissociation channel. These calculations focus on the electronic states of $^4\Sigma_u^-$ symmetry, which can be populated

[1]Barriers of some eV may be present in multicharged species [26,27].

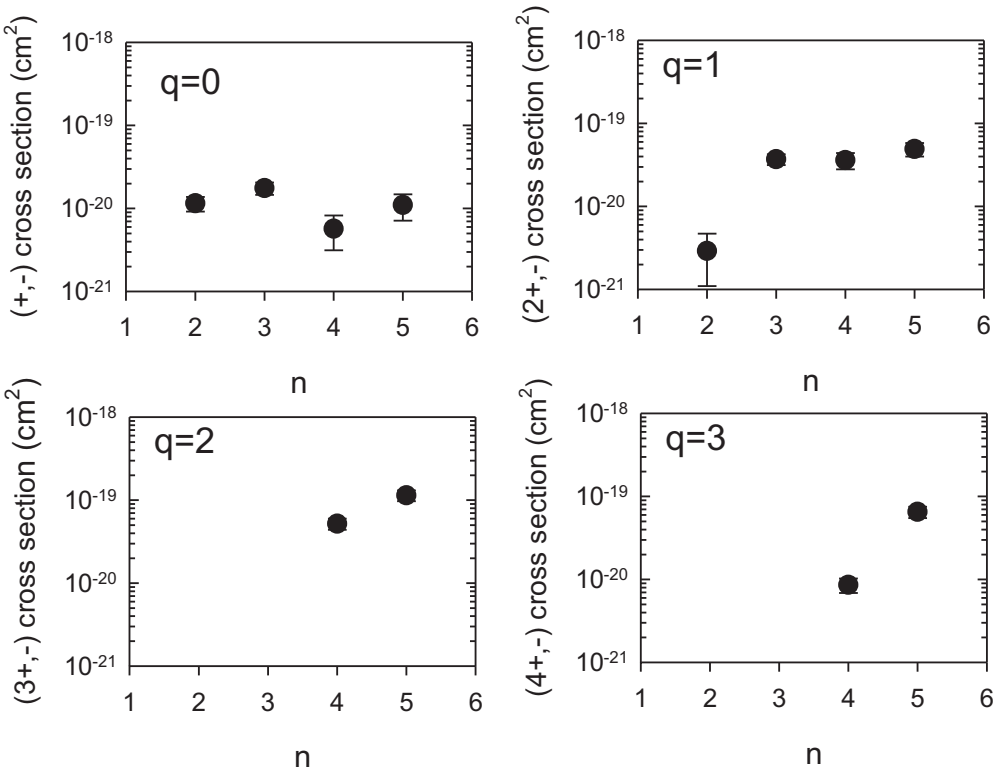

FIG. 3. Measured ion-pair dissociation cross sections $\sigma((q+1)+,-)$ of C_n^{q+} clusters as a function of n (abscissa) and for various q values (from top left to bottom right, $q = 0, 1, 2, 3$).

during the collision according to the dipole-transition rules detailed below. The potential-energy curves of the 25 lowest $^4\Sigma_u^-$ states have been calculated with the state-averaged complete active space self-consistent field method (CASSCF) [31,32] and the cc-pVTZ basis set using the MOLPRO package [33]. They are depicted in Fig. 5. Based on the Mulliken population analysis, we characterized the fundamental ionic channels of C^{2+}-C^- interacting with the valence electronic states of lower energies in a cascade of avoided crossings, as shown in the upper panel of Fig. 5 where only the $^4\Sigma_u^-$ states are represented.

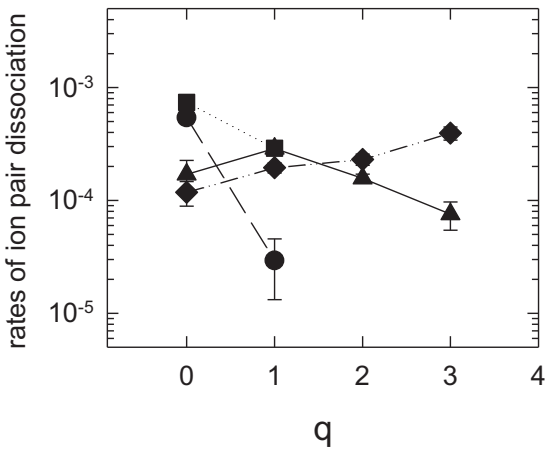

FIG. 4. Measured rates of ion-pair dissociation as compared with total dissociation of C_n^{q+} species as a function of q and for various n values: circles, squares, upward triangles, diamonds are for $n = 2$, 3, 4, 5, respectively. Lines are to guide the eye.

Let us note that states of $^4\Pi_u$ symmetry, not presented here, are also populated and thus increase the total number of states implied in the fragmentation dynamics. The analysis of the wave functions along the reactive coordinate allowed us to follow the progressive mixing of the ion-pair channel with the valence states and to approximate the corresponding diabatic path, represented in Fig. 5 by a dashed-dotted line.

Figure 5 clearly illustrates that the complexity of the molecular structure of C_2^+ and the highly excited states involved (well above the ionization energy of C_2^+ represented by a dotted blue line) make a quantitative study and following of the IPD process impossible to handle. Rather, due to the very large number of populated states in the entrance (collision) and exit (relaxation) channels we chose to interpret the results within a statistical (nondynamical) approach. In Sec. IV A the exact formulation of $R_{\rm IPD}$ as a function of the cluster internal energy E^* is given. The calculation of the cluster internal energy distribution after the collision, $f(E^*)$, is presented in Sec. IV B. The determination of $R_{\rm IPD}(E^*)$ within a simple statistical approach is presented in Sec. IV C. Results of the calculated $R_{\rm IPD}$ and comparison with the experimental values are presented in Sec. IV D.

A. Internal-energy-dependent expression of $R_{\rm IPD}$

Expressions of $R_{\rm IPD}$ in C_2^+ and C_3^+ have been given in Eqs. (1) and (5), respectively. It is obvious that $R_{\rm IPD}$ depends very much on the internal energy of the species E^*. Indeed, $R_{\rm IPD}$ is null as long as E^* is less than the energy threshold for IPD (called $E_{\rm IPT}$ in the following, where $E_{\rm IPT}$ is the energy of the less costly IPD channel within an (n,q) species) and

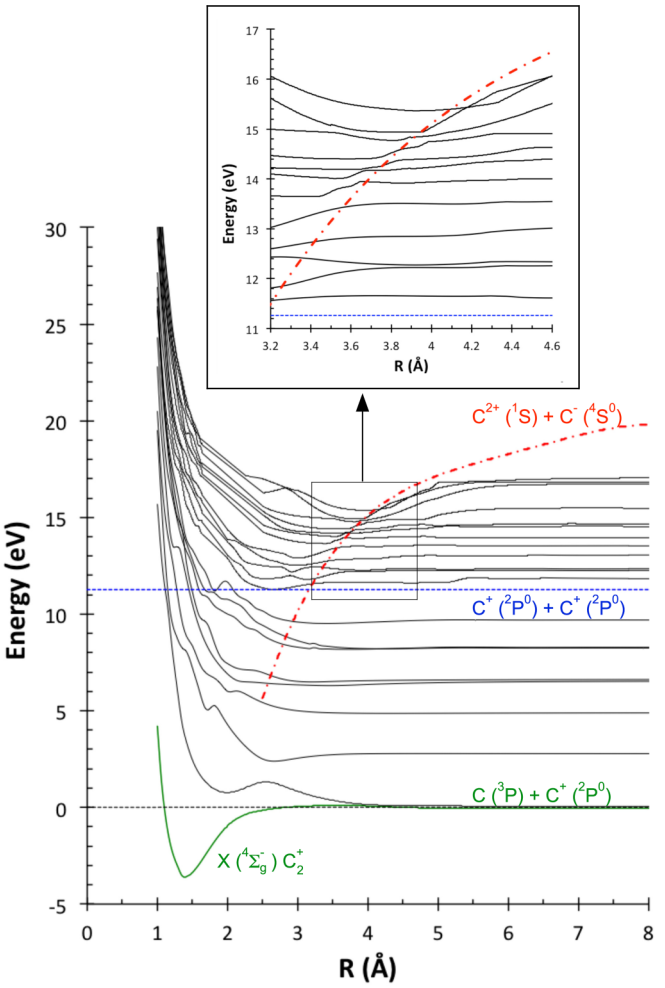

FIG. 5. Visualization of the PECs (in eV) of the 25 lowest $^4\Sigma_u^-$ states of C_2^+ from CASSCF *ab initio* calculations. The lowest C^{2+}-C^- ion-pair channel (dashed-dotted red line) undergoes a cascade of avoided crossings with the highly excited valence states of C_2^+, as detailed in the zoom on the interaction region. Lower-energy dissociation limits for C-C^+, C^+-C^+, and C^{2+}-C^- are highlighted in colors. The calculations were performed from 10.0 Å to 1.0 Å by steps of 0.01 Å except near avoiding crossings where the step was fixed to 0.001 Å.

R_{IPD} is expected to vary with E^* above E_{IPT} (opening of new channels) as will be confirmed later. Therefore, formulas depending on the internal energy of the fragmenting system seem appropriate. It is easy to show that, by using expressions such as those given for C_2^+ [Eqs. (1)–(3)] and expressing $\sigma_{\mathrm{exc.diss}}$ as a differential cross section with respect to E^*, it is possible to express R_{IPD} in a general way as

$$R_{\mathrm{IPD}} = \int_{E_{\mathrm{IPT}}}^{\infty} f(E^*) R_{\mathrm{IPD}}(E^*) dE^*, \tag{7}$$

with

$$f(E^*) = \frac{\frac{d\sigma_{\mathrm{exc.diss}}}{dE^*}}{\sigma_{\mathrm{exc.diss}}}, \tag{8}$$

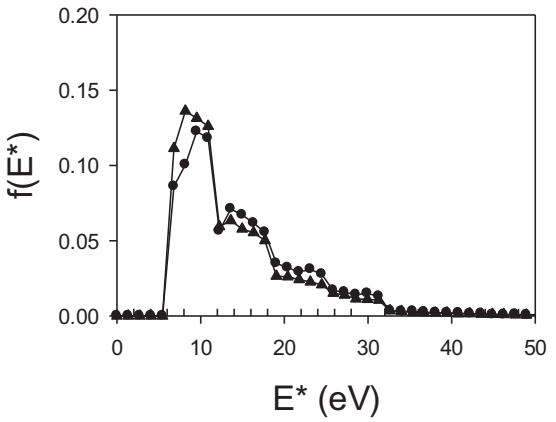

FIG. 6. Internal energy distribution of excited C_2^+ (circles) and C_3^+ (triangles) calculated with the IAE model.

and

$$\sigma_{\mathrm{exc.diss}} = \int_{E_{\mathrm{diss}}}^{\infty} \frac{d\sigma_{\mathrm{exc.diss}}}{dE^*} dE^*, \tag{9}$$

where $f(E^*)$ is the internal energy distribution of the system after dissociative electronic excitation and E_{diss} is the minimum internal energy for dissociative excitation (equal to 5.4 eV for C^+-C dissociation and 12 eV for C^+-C-C dissociation [23]). Note that Eq. (7) is an exact formulation of R_{IPD}. It applies to C_2^+ or C_3^+ if introducing the proper E_{IPT} (equal to 28.5 and 23.2 eV, respectively, see last column of Table I). A simple collision model was used to extract $f(E^*)$ in C_2^+ and C_3^+ (see Sec. IV B) whereas a statistical model was applied for the determination of $R_{\mathrm{IPD}}(E^*)$ as explained in Sec. IV C.

B. Internal energy distributions $f(E^*)$ of C_2^+ and C_3^+

In C_2^+ and C_3^+, IPD arises from relaxation of electronically excited clusters in the valence shell. Indeed, excitation in the inner shell, of much smaller cross section (around 10^{-18} cm^2 per carbon atom [34] as compared with 10^{-16} cm^2 in the valence shell), is followed, in 99.8% of the cases [34], by a rapid Auger effect of lifetime around a few fs [35], i.e., before dissociation occurs [12,13]. The internal energy distributions of C_2^+ and C_3^+ due to dissociative electronic excitation in valence shells have been calculated by using an independent atom and electron (IAE) model [36] together with classical trajectory Monte Carlo method (CTMC) for the calculation of the energy deposited in individual C and C^+ atoms. More details are given in Refs. [37,39]. In particular, we showed [37] that the obtained internal energy distributions allowed to reproduce the measured branching ratios of dissociation of C_n^+ clusters. In Fig. 6 are shown $f(E^*)$ obtained for C_2^+ and C_3^+ within this simple model. Structures are roughly associated with excitation of $2p$ electrons (lower-energy peak), $2s$ electrons (middle peaks), and double excitation (above 18 eV). It is readily seen that the part of excitation allowing dissociation into the ion pair ($E^* \geqslant E_{\mathrm{IPT}}$) is small, roughly 7% for C_2^+ ($E_{\mathrm{IPT}} = 28.5$ eV) and 13% for C_3^+ ($E_{\mathrm{IPT}} = 23.1$ eV). It is also seen that $f(E^*)$ becomes very small for E^* larger than 35 eV, which is going to be the highest energy considered in the calculation.

There are constraints about the molecular states that are populated during the collision. If we assume that dipole transitions dominate, which is indeed the case in high-velocity collisions [38], transitions from the initial molecular state must obey the following selection rules [40,41]: $\Delta S = 0$ (spin conservation), $\Delta\Lambda = 0,\pm 1$ (Λ is the projection along the internuclear axis of the electronic orbital angular momentum), $u \leftrightarrow g$ transition (symmetry with respect to the molecule symmetry center), and $\Sigma^+ \leftrightarrow \Sigma^-$ forbidden (symmetry with respect to a plane containing the internuclear axis). Starting from the C_2^+ ground state ($X\,^4\Sigma_g^-$) we populate final states of the $^4\Sigma_u^-$ and $^4\Pi_u$ symmetry whereas populated states from the C_3^+ ground state ($X\,^2\Sigma_u^+$) are of the $^2\Sigma_g^+$ and $^2\Pi_g$ types.

C. Calculation of $R_{\mathrm{IPD}}(E^*)$ within a statistical model

We want to calculate $R_{\mathrm{IPD}}(E^*)$, the probability that the excited system dissociates along an ion-pair channel rather than along "normal dissociation" (i.e., without anion emission). Dissociation of molecular states depends strongly on the considered state. As seen in Fig. 5, highly excited molecular states tend to correlate, adiabatically, to highly excited dissociation limits. But if we take into account the numerous crossings that take place between molecular states on the way to dissociation (nonadiabatic transitions) then a very large range of final states is open. The fact that dissociation from highly excited states may give rise to dissociation into low excited final states is confirmed from some experimental results. Indeed, following electronic excitation of C_2^+, peaked around 10 eV (see Fig. 6), we measured a kinetic-energy release (KER) in C^+-C fragmentation peaked around 3 eV, i.e., consistent with dissociation in the lowest-excited dissociation limit (5.4 eV for the first-dissociation limit; see Fig. 5). In this context our approach was to consider that, within the phase space of all possible final molecular states, they were all equiprobable.

As discussed in Sec. IV B, the available phase space is composed of molecular states having the proper symmetry, i.e., obeying the dipole selection rules from the initial electronic state. On the other hand, the conservation of energy imposes that molecular states are connected to dissociation limits situated below E^*. Expressions of $R_{\mathrm{IPD}}(E^*)$ in C_2^+ and C_3^+ are given in Eqs. (10) and (11), respectively. In Eq. (10) [Eq. (11)] $N_{\mathrm{mol.states}} \rightarrow C^{2+}\text{-}C^-$ ($N_{\mathrm{mol.states}} \rightarrow C^+\text{-}C^+\text{-}C^-$) refer to the number of molecular states having the proper symmetry and correlating to ion-pair dissociation limits situated below E^* and $N'_{\mathrm{mol.states}} \rightarrow C^+\text{-}C$ ($N'_{\mathrm{mol.states}} \rightarrow C^+\text{-}C\text{-}C$) to the number of molecular states having the proper symmetry and correlating to normal dissociation limits situated below E^*. For instance, in the simplistic case where there is only two normal dissociation limits (DL1 and DL2 with N_1 and N_2 being the number of molecular states connected to each) and one ion-pair-dissociation limit (DL3 with N_3 molecular states connected to it), $R_{\mathrm{IPD}}(E^*)$ is equal to $N_3/(N_1 + N_2 + N_3)$.

$$R_{\mathrm{IPD}}(E^*) = \frac{N_{\mathrm{mol.states}} \rightarrow \mathrm{C}^{2+}\text{-}\mathrm{C}^-}{N'_{\mathrm{mol.states}} \rightarrow C^+\text{-}C + N_{\mathrm{mol.states}} \rightarrow \mathrm{C}^{2+}\text{-}\mathrm{C}^-}, \tag{10}$$

for the case of C_2^+ dissociation and

$$R_{\mathrm{IPD}}(E^*) = \frac{N_{\mathrm{mol.states}} \rightarrow C^+\text{-}C^+\text{-}\mathrm{C}^-}{N'_{\mathrm{mol.states}} \rightarrow C^+\text{-}C\text{-}C + N_{\mathrm{mol.states}} \rightarrow C^+\text{-}C^+\text{-}\mathrm{C}^-}, \tag{11}$$

for the case of C_3^+ dissociation.

The E^* dependence of $R_{\mathrm{IPD}}(E^*)$ comes from the change in the number of accessible molecular states with E^*, either in the numerator (IPD states) or in the denominator. From a practical point of view the number of dissociation limits situated below E^* was first evaluated. Then the number of molecular states of proper symmetry correlating to each dissociation limit was calculated.

The first task is then to count the number of dissociation limits situated below E^*. These limits associate various C and C^+ terms ($^{2S+1}L^{(o)}$), a list of which can be found, for instance, in the NIST database [42]. One difficulty associated with the large $\Delta = (E^* - E_{\mathrm{diss}})$ domains that have to be considered ($\Delta_{\mathrm{min}} = 10$ eV in C_3^+ and $\Delta_{\mathrm{min}} = 23.1$ eV in C_2^+) is that an infinite number of dissociation limits are theoretically to be introduced as long as $\Delta \geqslant 11.26$ eV (Rydberg states $2p \rightarrow nl$ in C) and $\Delta \geqslant 24.38$ eV (Rydberg states in C^+). It is nevertheless expected that the contribution of high n values will decrease with n. Schiavone *et al.* [43] have shown, for instance, that the production of high-Rydberg (HR) atomic fragments in electron-impact dissociation of 13 molecules follows a $\frac{1}{n^3}$ dependence. These measurements were performed at 100 eV electron kinetic energy ($v_p = 2.7$ a.u.), a collision system very close to ours according to the Z_p/v_p criterion ($v_p = 2.25$ a.u. and Z_p(He)=1-2 depending on the impact parameter in the here studied systems). Since molecular Rydberg states are possibly contributing to IPD and since molecular Rydberg states are likely to dissociate into HR atomic fragments [44], the question arises of where to cut in n the countings. The IPD process representing roughly 10^{-4}

TABLE III. Ion-pair-dissociation limits situated in the 28.5–35 eV energy domain above the ground state of C_2^+. The number and type of molecular states converging to each limit and meeting the selection rules (see text and appendix) are given in the last column. The number of states of each type is given in parentheses. For the second ion-pair limit, molecular states populated from the metastable C_2^+ ($a\,^2\Pi_u$) are also reported.

Dissociation limits	Energy above C_2^+ ($X\,^4\Sigma_g^-$) (eV)	Molecular states (number)
$C^-(^4S^\circ)$-$C^{2+}(^1S)$	28.5	$^4\Sigma_u^-$ (1)
$C^-(^4S^\circ)$-$C^{2+}(^3P^\circ)$	35.0	$^4\Sigma_u^-$ (1), $^4\Pi_u$ (1)
	34.2 [above C_2^+ ($a\,^2\Pi_u$)]	$^2\Sigma_g^-$ (1), $^2\Pi_g$ (1) [from C_2^+ ($a\,^2\Pi_u$)]

TABLE IV. Same as Table III but for C_3^+.

Dissociation limits	Energy above C_3^+ ($X\,^2\Sigma_u^+$) (eV)	Molecular states (number)
$C^-(^4S^\circ)$-$C^+(^2P^\circ)$-$C^+(^2P^\circ)$	23	$^2\Sigma_g^+$ (1), $^2\Pi_g$ (3)
$C^-(^4S^\circ)$-$C^+(^2P^\circ)$-$C^+(^4P)$	28.5	$^2\Sigma_g^+$ (12), $^2\Pi_g$ (12)
$C^-(^4S^\circ)$-$C^+(^2P^\circ)$-$C^+(^2D)$	32.5	$^2\Sigma_g^+$ (3), $^2\Pi_g$ (9)
$C^-(^4S^\circ)$-$C^+(^4P)$-$C^+(^4P)$	33.6	$^2\Sigma_g^+$ (3), $^2\Pi_g$ (6)
$C^-(^4S^\circ)$-$C^+(^2P^\circ)$-$C^+(^2S)$	35	$^2\Sigma_g^+$ (0), $^2\Pi_g$ (3)

of the dissociative excitation cross section we see from the $\frac{1}{n^3}$ law that HR atomic fragments with n up to $n = 60$ could be considered. In the NIST database, terms up to $n = 30$ are typically included. To see the effect of the cut in n, we also made countings with $n = 20$ and $n = 10$.

The second task is to calculate the number of molecular states correlating to the various dissociation limits. For that we used the building-up principles given in Herzberg (1950) [40] for diatomics and Herzberg (1966) [41] for polyatomics. For C_2^+, the counting is rather straightforward using the Herzberg tables whereas the counting for C_3^+ is more complicated due to the permutation of the three identical carbon nuclei; see the appendix. The effect of the permutation has been taken into account exactly for the calculation of the number of ion-pair molecular states entering in the numerators of Eqs. (10) and (11) (and reported in Tables III and IV). The counting of states entering in the denominators of Eqs. (10) and (11) and associated with normal dissociation strictly follows the group theoretical treatment illustrated in the appendix for ion-pair channels. This leads to the introduction of multiplication factors resulting from permutational symmetry. For C_3^+, most of the C^+-C-C channels correspond to the case where both C atoms are in a different electronic state, which implies that a permutational multiplication factor of three applies to g or u selected states. Neglecting the occurrence of the rare channels in which both C atoms are in the same state, one can adopt the factor of three as a mean value for all molecular states emerging from C^+-C-C dissociation limits. Associated values are reported in Tables V and VI.

D. Ion-pair-dissociation rates in C_2^+ and C_3^+, comparison with experiment, and discussion

We give in Tables III and IV the ion-pair-dissociation limits which are in the energy domain between $E_{\rm IPT}$ and 35 eV together with the number and type of molecular states which are converging to these limits and are possibly populated

TABLE V. Normal dissociation in C_2^+: Number of dissociation limits of the C^+-C type ($N_{\rm diss}$) situated below 28.5 eV (column 2) and below 35 eV (column 3) as a function of the cut in n (see text). In columns 4 and 5 are reported the number of molecular states converging to these limits and allowed by selection rules ($N_{\rm mol}$).

	$N_{\rm diss}$ 28.5 eV	$N_{\rm diss}$ 35 eV	$N_{\rm mol}$ 28.5 eV	$N_{\rm mol}$ 35 eV
NIST	400	916	1508	3100
$n \leqslant 20$	383	880	1408	2955
$n \leqslant 10$	304	708	1206	2311

TABLE VI. Normal dissociation in C_3^+: Number of dissociation limits of the C^+-C-C type ($N_{\rm diss}$) situated below 23 eV (column 2) and below 35 eV (column 3) as a function of the cut in n (see text). In column 4 and 5 are reported the number of molecular states converging to these limits and allowed by selection rules ($N_{\rm mol}$).

	$N_{\rm diss}$ 23 eV	$N_{\rm diss}$ 35 eV	$N_{\rm mol}$ 23 eV	$N_{\rm mol}$ 35 eV
NIST	226	26 767	8631	1 303 374
$n \leqslant 20$	226	23 335	8631	1 000 608
$n \leqslant 10$	226	13 594	8631	572 085

according to the dipole selection rules. For C_2^+ (see Table III) we also made the counting starting from the $a\,^2\Pi_u$ metastable state since this state is likely to be present in the incoming beam[2] and since it leads to a very different IPD rate. Indeed, due to spin conservation, the first ion-pair-dissociation limit cannot be reached from C_2^+ ($a\,^2\Pi_u$) and only the second one, much higher in energy, can be populated.

In contrast with these few ion-pair-dissociation limits, the number of final states associated with a normal dissociation (of the C^+-C type for C_2^+, on the C^+-C-C type for C_3^+) is enormous (see Tables V and VI). On the basis of the NIST database, we identified 400 C^+-C limits situated below $E_{\rm IPT} = 28.5$ eV to which converge more than 1500 allowed molecular states; this number is doubled at $E^* = 35$ eV. For the case of C_3^+, the number of dissociation limits of the C^+-C-C type is more than 200 at $E^* = 23$ eV and close to 30 000 at $E^* = 35$ eV. This very large jump between $E^* = 23$ eV and $E^* = 35$ eV is due to the fact that, at the latter energy, two Rydberg series associated with the two carbon atoms contribute to the number of dissociation limits. Considering now the cuts at $n = 20$ and $n = 10$ we find a moderate effect in C_2^+ whereas the larger effect is seen in C_3^+ at $E^* = 35$ eV, originating from the double cut on the two Rydberg series. But the overall effect on the IPD rate remains small because this energy does not contribute much.

On the basis of these countings, $R_{\rm IPD}(E^*)$ [Eqs. (10) and (11)] were calculated for three E^* values: 28.5, 33.5, and 35 eV for C_2^+ [$R_{\rm IPD}(E^*)$, respectively equal to 6.6×10^{-4}, 4.1×10^{-4}, and 9.7×10^{-4}], 23, 28.5, and 35 eV for C_3^+ [$R_{\rm IPD}(E^*)$, respectively equal to 4.6×10^{-4}, 7.1×10^{-4}, and 4.0×10^{-5}]. The integrated rates $R_{\rm IPD}$ were then obtained by using Eq. (7) where integration by parts was done over the three values of E^*.

Results for the calculated rates and comparison with the experimental rates are given in Table VII. As seen from Table VII the model furnishes the right order of magnitude for $R_{\rm IPD}$. This means that the relative number of final molecular states connected to ion-pair-dissociation limits is indeed important in this matter. The very good agreement between the model and the experimental result for C_2^+ ($X\,^4\Sigma_g^-$) is probably accidental because we do not expect the model to be so accurate. Relative values are more meaningful. We note that

[2] C_2^+ is formed by stripping, at the accelerator terminal, of two electrons from C_2^-. Removal of two more external electrons from C_2^- (ground state) leads to C_2^+ ($a\,^2\Pi_u$).

TABLE VII. Comparison between measured and predicted R_{IPD}. Experimental R_{IPD} are those of Fig. 4 ($n = 2$–3, $q = 1$); calculated R_{IPD} were obtained by using Eq. (7).

Initial state	Calculated R_{IPD} NIST	Calculated R_{IPD} n $\leqslant$ 20	Calculated R_{IPD} $n \leqslant 10$	Experimental R_{IPD} (rel. error)
C_2^+ ($X\,^4\Sigma_g^-$)	3.0×10^{-5}	3.2×10^{-5}	3.9×10^{-5}	3.0×10^{-5} (60%)
C_2^+ ($a\,^2\Pi_u$)	8.7×10^{-6}	9.0×10^{-6}	1.1×10^{-5}	
C_3^+ ($X\,^2\Sigma_u^+$)	5.6×10^{-5}	5.9×10^{-5}	7.0×10^{-5}	5.3×10^{-4} (30%)

the R_{IPD} do not depend strongly on the cut in n. For C_2^+ we have a sizable lowering of the rate when considering the molecule in a metastable state instead of in the ground state, but unfortunately the experimental contribution of the former one is unknown. We observe that predicted R_{IPD} are larger in C_3^+ than in C_2^+, as in the experiment. This results can be explained by two factors: First, the density of ion-pair states is much smaller in C_2^+ than in C_3^+ (a factor 15 in the [28.5, 35] eV energy domain); this will play a role, for instance, in the [33.5, 35] eV range in C_2^+ where there is no ion-pair limit at all. Second, the E_{IPT} value is much higher in C_2^+ (28.5 eV) than in C_3^+ (23 eV). This energy cost reduces roughly by a factor two the excitation probability above E_{IPT} in C_2^+ as compared with C_3^+, on the basis of the $f(E^*)$ function. Both phenomena have their origin in the fact that a C^{2+} fragment is emitted in IPD of C_2^+ and not in IPD of C_3^+. The same explanation is probably at the origin of the lower IPD rate for C_4^{3+} as compared with C_5^{3+} (see Table I).

Interestingly enough, the application of this statistical approach to the systems studied by Tabet *et al.* (H_3^+, H_2-He collisions at $v = 1.4$ a.u. [9]) leads to similar conclusions. Performing $R_{IPD}(E^*)$ calculations at the threshold energy for IPD ($E_{IPT} = 17.5$ eV for H^+-H^- [45] and $E_{IPT} = 22.20$ eV for H^+-H^+-H^- [6] and taking $R_{IPD}(E^*)$ constant over the whole $f(E^*)$ distribution above $E^* = E_{IPT}$ [with $f(E^*)$ also calculated within the IAE model], we obtained approximate R_{IPD} values reported in Table VIII and compared with both the experiment and the C_3^+ result. As seen in Table VIII, the statistical approach is also furnishing too-low values for H_3^+ and H_2 as compared with the experiment, but the ordering of R_{IPD}, from the lowest value in the case of C_3^+ up to the largest value for H_2, is preserved. This indicates that there is a clear correlation between R_{IPD} and the relative number of final states connecting to ion-pair and normal dissociation limits, respectively. On the other hand, the assumption of equal weight for all molecular states situated below E^* leads to a too-large number of states for normal dissociation and, accordingly, too-low R_{IPD} values predicted by the model.

TABLE VIII. Comparison between measured and predicted R_{IPD} for C_3^+, H_3^+, and H_2. Experimental R_{IPD} for H_3^+ giving rise to H^+-H^+-H^- and H_2 giving rise to H^+-H^- in $v = 1.4$ a.u. H_3^+ and H_2-He collisions were measured by Tabet *et al.* [9].

Initial state	Calculated R_{IPD}	Experimental R_{IPD} (rel. error)
C_3^+	0.56×10^{-4}	5.3×10^{-4} (30%)
H_3^+	0.22×10^{-3}	1.7×10^{-3} (40%)
H_2	0.13×10^{-2}	1.2×10^{-2} (50%)

V. CONCLUSION AND PERSPECTIVES

In conclusion, we have measured the ion-pair-dissociation cross sections of carbon clusters C_n^{q+} of various masses ($n = 2$–5) and charges ($q = 0$–3). Highly excited and ionized species were formed by high-velocity collisions between C_n^+ clusters and helium atoms ($v = 2.25$ a.u., $n = 1$–5). By performing coincidences between anionic and cationic fragments it was possible to resolve all ion-pair dissociation channels of a given (n,q) species. As compared with normal dissociation without anionic emission, it was found that the small IPD rates (of the order of 10^{-4}) were almost constant with n and q with the notable exception of C_2^+ giving rise to C^{2+}-C^- fragments about ten times smaller than the IPD of C_3^+ giving C^+-C^+-C^- fragments. We tentatively interpreted C_2^+ and C_3^+ IPD rates by applying a statistical model based on the main approximation that these rates are proportional to the relative number of accessible final molecular states at infinite distances. Despite these crude approximations, it was possible to find the right order of magnitude for the IPD rates in C_2^+ and C_3^+ and to explain qualitatively the lower value obtained in the former case. The ability of the approach to predict relative magnitudes of R_{IPD} in different systems was further demonstrated by results of R_{IPD} calculations for H_3^+ and H_2 excited in high-velocity collisions and measured by Tabet *et al.* [9].

As to perspectives, the question arises of whether this model could be applied to interpret the results of the other C_n^{q+} clusters. Considering first the higher sizes ($n = 3$–4) we are confronted to a number of final states to be enumerated which becomes enormous and, in light of previous results, probably too large. In that respect it would help to go beyond the assumption of equally probable final molecular states. This would imply finding some propensity rules applicable to the dissociation of highly excited molecules. Concerning clusters of different charge states ($q = 0, 2, 3$), we have some information about the energy deposited by electron capture ($q = 0$) and by ionization ($q \geqslant 2$) [29,39], but no indication at all as to the type of molecular states that are populated. Then again the number of molecular states considered in a counting may be much too large. Possible directions for the future could be to extract information from *individual* ion-pair-dissociation channels that have not been exploited so far [only R_{IPD}, the sum of the channels within an (n,q) species was interpreted]. Also it could be of interest to study IPD in other systems. We recently measured IPD in C_nN^+ clusters instead of C_n^+ projectiles. The first results for $n = 1$ indicate sizeably lower

IPD rates for identical electron capture, dissociative electronic excitation, and ionization cross sections. The whole n series ($n = 1$–4) will be studied and analyzed in the near future.

ACKNOWLEDGMENTS

T.L. acknowledges a FRIA grant of the F.R.S.-FNRS of Belgium. The ULB team acknowledges financial support from the IISN and PdR programs from the F.R.S.-FNRS. Financial support for the Orsay-Bruxelles collaboration has been provided by the GDR EMIE of the Centre National de la Recherche Scientifique.

APPENDIX: GROUP THEORETICAL TREATMENT

This appendix explains the group theoretical treatment which has been used for deriving the type and respective number of molecular states correlating to ion-pair dissociation channels reported in Tables III and IV. The procedure will first be presented by using C_2^+ as an example. It will then be applied to linear C_3^+ in which two different coupling cases occur.

1. $C^-(^4S^\circ) + C^{2+}(^3P^\circ) \longrightarrow C_2^+$

Applying the Wigner–Witmer diatomic correlation rules for unlike atomic fragments C^- and C^{2+} (see Table 26 of Herzberg's book [40]) and performing the spin coupling leads to the resulting $C_{\infty v}$ molecular states:

$$^2\Sigma^-,\ ^2\Pi,\ ^4\Sigma^-,\ ^4\Pi,\ ^6\Sigma^-,\ ^6\Pi. \tag{A1}$$

Note that, for spatial symmetry, the same result is obtained from a direct product adapted to $C_{\infty v}$ symmetry: $\Sigma^-(S^\circ) \times (\Sigma^+ + \Pi)(P^\circ) \rightarrow \Sigma^- + \Pi$.

The results (A1) do not, however, take into account the fact that, while fragments with different numbers of electrons are unlike, they have nevertheless identical nuclei. It follows that C_2^+ is an homonuclear system possessing $D_{\infty h}$ inversion symmetry. As inversion transforms a function centered on one nucleus to the same function on the other one, it is necessary to build the eigenfunctions of C_2^+ at the dissociation limit as linear combinations of the two degenerate wave functions differing by a permutation of the two identical carbon nuclei numbered 1 and 2:

$$\Psi_\pm = \frac{1}{\sqrt{2}}\{[\Psi(C^-(^4S^\circ);1) \times \Psi(C^{2+}(^3P^\circ);2)] \pm [\Psi(C^-(^4S^\circ);2) \times \Psi(C^{2+}(^3P^\circ);1)]\}. \tag{A2}$$

These functions maintain the spin and $C_{\infty v}$ characters of (A1), but are also eigenfunctions of the molecular inversion operator, with characters g and u for Ψ_+ and Ψ_-, respectively. The final result is thus

$$C^-(^4S^\circ) + C^{2+}(^3P^\circ) \longrightarrow {}^2\Sigma_g^-,\ ^2\Pi_g,\ ^4\Sigma_g^-,\ ^4\Pi_g,\ ^6\Sigma_g^-,\ ^6\Pi_g \text{ and } {}^2\Sigma_u^-,\ ^2\Pi_u,\ ^4\Sigma_u^-,\ ^4\Pi_u,\ ^6\Sigma_u^-,\ ^6\Pi_u, \tag{A3}$$

among which only some of the states obey the selection rules (see Table III).

2. $C^-(^4S^\circ) + C^+(^2P^\circ) + C^+(^4P) \longrightarrow C_3^+$

All participating ion-pair dissociation limits of C_3^+ correspond to C^--C^+-C^+ channels, and in the present case the two identical C^+ fragments are in different electronic states. As in the case of C_2^+, while fragments C^- and C^+ are unlike, molecular states arise from three identical carbon nuclei and belong to the $D_{\infty h}$ point group. Note that the middle fragment is centered at the inversion point and already possesses the molecular g or u symmetry.

Six degenerate uncoupled fragment wave functions can be built, each differing by a permutation of the three identical carbon nuclei:

$$\Psi_{ijk} = \Psi(C^-(^4S^\circ);i) \times \Psi(C^+(^2P^\circ);j) \times \Psi(C^+(^4P);k), \tag{A4}$$

with $ijk = 123, 213, 132, 231, 312$, and 321, defining the numbering of the nuclei.

The total degeneracy of this channel is very high ($6 \times 288 = 1728$). Each wave function in Eq. (A4) leads to the same resulting $C_{\infty v}$ states, resulting from the $C_{\infty v}$ adapted direct product or from the Wigner–Witmer rules extended to linear polyatomic molecules (see Table 22 of Herzberg [41]):

$$^{2,4,6}[\Sigma^+(4),\ \Sigma^-(2),\ \Pi(4),\ \Delta(2)] + {}^8[\Sigma^+(2),\ \Sigma^-(1),\ \Pi(2),\ \Delta(1)]. \tag{A5}$$

Eigenfunctions of the molecular inversion operator are obtained by projecting Eq. (A4) functions on the irreducible representations (IRs) A_g and A_u of the inversion group C_i, leading to linear combinations of three couples of Ψ_{ijk} functions:

$$\begin{aligned}\Psi_{1\pm} &= \frac{1}{\sqrt{2}}[\Psi_{123} \pm \Psi_{321}],\\ \Psi_{2\pm} &= \frac{1}{\sqrt{2}}[\Psi_{132} \pm \Psi_{312}],\\ \Psi_{3\pm} &= \frac{1}{\sqrt{2}}[\Psi_{213} \pm \Psi_{231}].\end{aligned} \tag{A6}$$

For all of these eigenfunctions, the symmetric and antisymmetric products of the atomic functions on nuclei 1 and 3 are g and u, respectively, but the function on the central nucleus 2 is g or u, depending on its atomic parity. It follows that Ψ_{1-}, Ψ_{2+}, Ψ_{3-} are g and Ψ_{1+}, Ψ_{2-}, Ψ_{3+} are u. The final result is that all $C_{\infty v}$ of Eq. (A5) occur three times with g and three times with u symmetry. States meeting the selection rule are $^2\Sigma_g^+(12)$ and $^2\Pi_g(12)$.

3. $C^-(^4S^\circ) + C^+(^2P^\circ) + C^+(^2P^\circ) \longrightarrow C_3^+$

The second case to consider for C_3^+ is when both C^+ ions are in the same state. Only three different degenerate uncoupled fragment wave functions appear in this case (identical C^+ are not exchanged):

$$\Psi_{ijk} = \Psi(C^-(^4S^\circ);i) \times \Psi(C^+(^2P^\circ);j) \times \Psi(C^+(^2P^\circ);k), \tag{A7}$$

with $ijk = 123$, 213, and 321.

The projection of Eq. (A7) functions on IRs of C_i tell us that Ψ_{213} already belongs to $D_{\infty h}$ and that a linear combination

is formed with the two remaining functions:

$$\Psi_{\pm} = \frac{1}{\sqrt{2}}[\Psi_{123} \pm \Psi_{321}]. \tag{A8}$$

$C_{\infty v}$ states arising from Ψ_{123} or Ψ_{321} are obtained as before from the Herzberg Tables [41]:

$$^2[\Sigma^+,\ \Sigma^-(2),\ \Pi(2),\ \Delta], \quad ^4[\Sigma^+(2),\ \Sigma^-,\ \Pi(4),\ \Delta(2)],$$
$$^6[\Sigma^+,\ \Sigma^-(2),\ \Pi(2),\ \Delta] \tag{A9}$$

All these states exist with additional g and u characters for Ψ_- and Ψ_+, respectively.

States of $D_{\infty h}$ symmetry resulting from Ψ_{213} do not occur in g, u pairs. The group theoretical treatment is different from previous ones. One must first couple both identical fragments together using the same rules as those that apply to an homonuclear diatomic molecule formed from identical $^2P^\circ$ states (see Table 28 of Ref. [40]):

$$^1[\Sigma_g^+(2),\ \Sigma_u^-,\ \Pi_g,\ \Pi_u,\ \Delta_g], \quad ^3[\Sigma_u^+(2),\ \Sigma_g^-,\ \Pi_g,\ \Pi_u,\ \Delta_u]. \tag{A10}$$

Noting that the g and u symmetry is governed by the antisymmetry of the total electronic eigenfunctions including the spin part. All states of (A10) must then be coupled to the $^4S^\circ$ state of C^-, which transforms to $^4\Sigma_u^-$ symmetry under $C_{\infty v}$ transformation, leading to

$$^{2,4,6}[\Sigma_g^-(2),\ \Sigma_u^+,\ \Pi_g,\ \Pi_u,\ \Delta_g],$$
$$^4[\Sigma_u^-(2),\ \Sigma_g^+,\ \Pi_g,\ \Pi_u,\ \Delta_u]. \tag{A11}$$

States arising from the $C^-(^4S^\circ) + C^+(^2P^\circ) + C^+(^2P^\circ)$ channel result from the sum of (A9) g,u pairs and (A11), from which only one $^2\Sigma_g^+$ and three $^2\Pi_g$ states meet the selection rule.

[1] R. Locht and J. Momigny, Int. J. Mass Spectrom. Ion Phys. **7**, 121 (1971).
[2] A. G. Suits and J. W. Hepburn, Annu. Rev. Phys. Chem. **57**, 431 (2006).
[3] M. J. Simpson and R. P. Tuckett, Int. Rev. Phys. Chem. **30**, 197 (2011).
[4] S. X. Tian, Phys. Chem. Chem. Phys. **14**, 6433 (2012).
[5] W. Zong, G. H. Dunn, N. Djurić, M. Larsson, C. H. Greene, A. Al-Khalili, A. Neau, A. M. Derkatch, L. Vikor, W. Shi, A. Le Padellec, S. Rosén, H. Danared, and M. af Ugglas, Phys. Rev. Lett. **83**, 951 (1999).
[6] O. Yenen, D. H. Jaecks, and L. M. Wiese, Phys. Rev. A **39**, 1767 (1989).
[7] M. Farizon, N. V. de Castro Faria, B. Farizon-Mazuy, and M. J. Gaillard, Phys. Rev. A **45**, 179 (1992).
[8] M. Barbatti, L. P. G. de Assis, G. Jalbert, L. F. S. Coelho, I. Borges, and N. V. de Castro Faria, Phys. Rev. A **59**, 1988 (1999).
[9] J. Tabet, S. Eden, F. Gobet, B. Farizon, M. Farizon, S. Ouaskit, P. Scheier, and T. D. Märk, Int. J. Mass Spectrom. **272**, 48 (2008).
[10] J.-Y. Chesnel, Z. Juhász, E. Lattouf, J. A. Tanis, B. A. Huber, E. Bene, S. T. S. Kovács, P. Herczku, A. Méry, J.-C. Poully, J. Rangama, and B. Sulik, Phys. Rev. A **91**, 060701 (2015).
[11] G. Dujardin, L. Hellner, B. J. Olsson, M. J. Besnard-Ramage, and A. Dadouch, Phys. Rev. Lett. **62**, 745 (1989).
[12] E. Rühl and R. Flesch, J. Chem. Phys. **121**, 5322 (2004).
[13] L. H. Coutinho, D. J. Gardenghi, A. S. Schlachter, G. G. B. de Souza, and W. C. Stolte, J. Chem. Phys. **140**, 024314 (2014).
[14] W. C. Stolte, M. M. Sant'Anna, G. Öhrwall, I. Dominguez-Lopez, M. N. Piancastelli, and D. W. Lindle, Phys. Rev. A **68**, 022701 (2003).
[15] A. V. Baklanov, L. M. C. Janssen, D. H. Parker, L. Poisson, B. Soep, J.-M. Mestdagh, and O. Gobert, J. Chem. Phys. **129**, 214306 (2008).
[16] S. M. Poullain, K. Veyrinas, P. Billaud, M. Lebech, Y. J. Picard, R. R. Lucchese, and D. Dowek, J. Chem. Phys. **139**, 044311 (2013).
[17] C. Elkharrat, Y. J. Picard, P. Billaud, C. Cornaggia, D. Garzella, M. Perdrix, J. C. Houver, R. R. Lucchese, and D. Dowek, J. Phys. Chem. A **114**, 9902 (2010).
[18] K. Béroff, M. Chabot, G. Martinet, T. Pino, S. Bouneau, A. Le Padellec, G. Féraud, N. D. Thi, F. Calvo, C. Bordas, and F. Lépine, J. Phys. B: At., Mol. Opt. Phys. **46**, 015201 (2013).
[19] K. Wohrer, M. Chabot, R. Fossé, and D. Gardès, Rev. Sci. Instrum. **71**, 2025 (2000).
[20] M. Chabot, S. Della Negra, L. Lavergne, G. Martinet, K. Wohrer-Béroff, R. Sellem, R. Daniel, J. Le Bris, G. Lalu, D. Gardès, J. A. Scarpaci, P. Désesquelle, and V. Lima, Nucl. Instrum. Methods Phys. Res., Sect. B **197**, 155 (2002).
[21] M. Chabot, G. Martinet, K. Béroff, T. Pino, S. Bouneau, B. Genolini, X. Grave, K. Nguyen, C. le Gailliard, P. Rosier, G. Féraud, H. Friha, and B. Villier, Rev. Sci. Instrum. **82**, 103301 (2011).
[22] A. Jallat, Ph.D. thesis, Université Paris Sud, 2015 (unpublished).
[23] S. Díaz-Tendero, G. Sánchez, P.-A. Hervieux, M. Alcamí, and F. Martín, Braz. J. Phys. **36**, 529 (2006).
[24] G. Sánchez-Sanz, S. Díaz-Tendero, F. Martín, and M. Alcamí, Int. J. Mass Spectrom. **299**, 20 (2011).
[25] J. C. Rienstra-Kiracofe, G. S. Tschumper, H. F. Schaefer, S. Nandi, and G. B. Ellison, Chem. Rev. (Washington, DC, U. S.) **102**, 231 (2002).
[26] H. Hogreve, J. Chem. Phys. **102**, 3281 (1995).
[27] H. Hogreve, J. Mol. Struct.: THEOCHEM **532**, 81 (2000).
[28] G. Martinet, S. Diaz-Tendero, M. Chabot, K. Wohrer, S. Della Negra, F. Mezdari, H. Hamrita, P. Desesquelles, A. Le Padellec, D. Gardes, L. Lavergne, G. Lalu, X. Grave, J. Clavelin, P. Hervieux, M. Alcami, and F. Martin, Phys. Rev. Lett. **93**, 063401 (2004).
[29] M. Chabot, G. Martinet, F. Mezdari, S. Diaz-Tendero, K. Béroff-Wohrer, P. Désesquelles, S. Della-Negra, H. Hamrita, A. Le Padellec, T. Tuna, L. Montagnon, M. Barat, M. Simon, and I. Ismaïl, J. Phys. B: At., Mol. Opt. Phys. **39**, 2593 (2006).
[30] F. Mezdari, Ph.D. thesis, University Paris VI, 2005 (unpublished).

[31] H.-J. Werner and P. J. Knowles, J. Chem. Phys. **82**, 5053 (1985).
[32] P. J. Knowles and H.-J. Werner, Chem. Phys. Lett. **115**, 259 (1985).
[33] H.-J. Werner, P. J. Knowles, G. Knizia, F. R. Manby, and M. Schütz, Wiley Interdiscip. Rev. Comput. Mol. Sci. **2**, 242 (2012).
[34] L. H. Toburen, R. D. DuBois, C. O. Reinhold, D. R. Schultz, and R. E. Olson, Phys. Rev. A **42**, 5338 (1990).
[35] K. Béroff, N. T. Van-Oanh, M. Chabot, T. Tuna, T. Pino, G. Martinet, A. Le Padellec, Y. Carpentier, and L. Lavergne, Phys. Rev. A **84**, 032705 (2011).
[36] K. Wohrer, M. Chabot, J. P. Rozet, D. Gard'es, D. Vernhet, D. Jacquet, S. D. Negra, A. Brunelle, M. Nectoux, M. Pautrat, Y. L. Beyec, P. Attal, and G. Maynard, J. Phys. B: At., Mol. Opt. Phys. **29**, L755 (1996).
[37] M. Chabot, F. Mezdari, G. Martinet, K. Wohrer-Beroff, S. Della Negra, P. Desesquelles, H. Hamrita, A. Le Padellec, and L. Montagnon, in *Fragmentation of Small Carbon Clusters*, in Photonic, Electronic and Atomic Collisions, edited by P. D. Fainstein, M. A. P. Lima, J. A. Miraglia, E. C. Montenegro, and R. D. Rivarola (World Scientific, Singapore, 2006), pp. 607–614.
[38] E. Merzbacher, NATO Advanced Science Institutes Ser. B **103**, 319 (1983).
[39] K. Béroff, M. Chabot, F. Mezdari, G. Martinet, T. Tuna, P. Désesquelles, A. Le Padellec, and M. Barat, Nucl. Instrum. Methods Phys. Res., Sect. B, **267**, 866 (2009).
[40] G. Herzberg, *Molecular Spectra and Molecular Structure, I. Spectra of Diatomic Molecules* (Van Nostrand Rheinhold, Princeton, 1950).
[41] G. Herzberg, *Molecular Spectra and Molecular Structure III, Electronic Spectra and Electronic Structure of Polyatomic Molecules* (Van Nostrand Rheinhold, Princeton, 1966).
[42] A. Kramida, Yu. Ralchenko, J. Reader, and NIST ASD Team, *NIST Atomic Spectra Database*, Ver. 5.3 (2015), http://physics.nist.gov/asd.
[43] J. A. Schiavone, S. M. Tarr, and R. S. Freund, J. Chem. Phys. **70**, 4468 (1979).
[44] A. Ehresmann, P. V. Demekhin, W. Kielich, I. Haar, M. A. Schlueter, V. L. Sukhorukov, and H. Schmoranzer, J. Phys. B: At. Mol. Opt. Phys. **42**, 165103 (2009).
[45] M. O. Vieitez, T. I. Ivanov, E. Reinhold, C. A. de Lange, and W. Ubachs, Phys. Rev. Lett. **101**, 163001 (2008).